

Article

# Material and Performance Optimisation for Syngas Preparation Using Artificial Intelligence (AI)-Based Machine Learning (ML)

Murphy M. Peksen

Chair of Energy Systems, TUM School of Engineering and Design, Technical University of Munich, Boltzmannstr 15, 85748 Garching bei Munich, Germany; m.peksen@tum.de

**Abstract:** Working towards a more sustainable future with zero emissions, the International Future Laboratory for Hydrogen Economy at the Technical University of Munich (TUM) exhibits concerted efforts across various hydrogen technologies. The current research focuses on pre-reforming processes for high-quality reversible solid oxide cell feedstock preparation. An AI-based machine learning model has been developed, trained, and deployed to predict and optimise the controlled utilisation of methane gas. Using a blend of design of experiments and a validated 3D computational fluid dynamics model, pre-reforming process data have been generated for various syngas mixtures. The results of this study indicate that it is possible to achieve a targeted methane utilisation rate of 20% while decreasing the amount of catalyst material by 11%. Furthermore, it was found that precise process parameters could be determined efficiently and with minimal resource consumption in order to achieve higher methane fuel utilisation rates of 25% and 30%. The machine learning model has been effectively employed to analyse and optimise the fuel outlet conditions of the pre-reforming process, contributing to a better understanding of high-quality syngas preparation and furthering sustainable research efforts for a safe reversible solid oxide cell (r-SOC) process.

**Keywords:** hydrogen; machine learning; sustainability; artificial intelligence; solid oxide cell; r-SOC; pre-reforming; syngas



**Citation:** Peksen, M.M. Material and Performance Optimisation for Syngas Preparation Using Artificial Intelligence (AI)-Based Machine Learning (ML). *Hydrogen* **2023**, *4*, 474–492. <https://doi.org/10.3390/hydrogen4030032>

Academic Editor: Daniel Hissel

Received: 5 June 2023

Revised: 26 June 2023

Accepted: 21 July 2023

Published: 25 July 2023



**Copyright:** © 2023 by the author. Licensee MDPI, Basel, Switzerland. This article is an open access article distributed under the terms and conditions of the Creative Commons Attribution (CC BY) license (<https://creativecommons.org/licenses/by/4.0/>).

## 1. Introduction

Solid oxide cell technologies, along with their auxiliary system attributes and processes, have emerged as a key research field in hydrogen technologies. With the increasing demand for hydrogen fuel generation, delivery, and utilisation, solid oxide fuel cell technology has garnered significant attention from researchers worldwide [1–13]. Over the last decade, numerous research groups have conducted investigations in this field, resulting in a plethora of success stories. These include experimental assessment of both individual components [8,14–22] and complete systems, with a focus on system integration, durability, and efficiency [7,12,22–29]. Computational modelling has also played a significant role in this research, with numerous studies utilising modelling techniques to provide insights into performance and system design aspects [30–35]. As research continues in several areas, it is anticipated that the cost structure of solid oxide cell systems will change rapidly, leading to reductions in the cost of balance-of-plant components and increasing their competitiveness by reducing the price per kWh. The ultimate cost of solid oxide cell systems will depend on various factors, including the chosen system size, application area, and market conditions.

Solid oxide cell (SOC) technology is an attractive choice as it can be used both as fuel cell and as an electrolyzer. Numerous scholars have been researching the implications of reversed solid oxide cell (r-SOC) capable fuel gas generation [36–41]. Another advantage of the technology is its fuel flexibility; it is able to utilise hydrogen as well as other hydrocarbon-containing sources in liquid and gas form [42–44]. Renewable biomass is an appealing fuel source that may also be used. SOC can process mixtures consisting of H<sub>2</sub>, H<sub>2</sub>, CO, CO<sub>2</sub>, and CH<sub>4</sub> species where more complex hydrocarbons, H<sub>2</sub>O, and tar, can also

be present and may require pre-cleaning [45–51]. Gasification is also a practical method that can convert carbonaceous substances into gaseous mixtures, i.e., in the form of syngas. These substances can be converted into syngas [41–44,52–59]. It should be noted that the gas composition is dependent on several factors, such as the obtained feedstock, the chosen gasification method and process conditions, and the catalyst properties.

Safe and efficient operation of solid oxide cell technology requires the removal of impurities from the fuel stream. In this context, the reforming process proves to be an effective means of pre-cleaning product streams of varying compositions, resulting in syngas that is pure enough to sustain seamless SOFC operation [56,60–62]. Pre-reforming of fuel is essential to mitigate safety issues and prevent material degradation that may arise when oxygen-rich fuel is released into a solid oxide fuel cell (SOFC). Moreover, control of the amount of methane feed reformed in the stack is necessary to ensure proper cooling of the fuel cell stack. These factors have led to the growing popularity of syngas production and utilisation via pre-reforming, particularly from a hydrogen economy perspective. In the field of solid oxide fuel cell (SOFC) technology, both computational methods and experimental measurements have been successfully employed to predict the performance of thermochemical reforming in integrated SOFC systems and to ensure the quality of fuel for efficient SOFC operation [17,60,63–71]. Numerical models validated through experimental measurements have proven effective in predicting and simulating the thermochemical reforming performance of integrated solid oxide fuel cell (SOFC) systems. Traditional methods such as the finite volume and finite element methods have been widely used, offering a robust and flexible tool for accurate results. These models have been successfully applied in various related applications, demonstrating their reliability and versatility [72–76]. Advanced, modern accelerated modelling approaches, empowered by Artificial Intelligence (AI), have gained popularity for their ability to dramatically improve the accuracy of predictions while also reducing the time required for modelling. By utilising AI-powered techniques, research can now achieve optimal outcomes quickly and efficiently. The flexibility and robustness offered by AI-based numerical models make them a powerful tool for predicting and simulating complex systems [77–83]. Previous research has demonstrated the significant benefits of utilising the design of experiments (DoE) in conjunction with studies of solid oxide technologies. This powerful approach has proven to be effective in providing valuable insights into the design and performance of these technologies. The authors have similarly employed this method, resulting in a deep understanding of solid oxide systems and their optimisation for enhanced efficiency and cost-effectiveness [64,84] and have recently extended its wide use coupled with Artificial Intelligence-based Machine Learning models [85].

With the exponential growth in the use of Artificial Intelligence (AI), sophisticated modelling approaches are revolutionising various research fields. AI systems offer great scalability and numerous prediction options, enabling the handling of large data sets generated by experimentally validated multiphysics models. The ability to understand complex processes and interactions precisely, without analysing huge multiphysics data sets individually, is one of the hallmarks of AI. This study harnesses the power of AI to optimise the fuel utilisation of methane, introducing various syngas constellations into a pre-reformer that can be externally connected to a solid oxide cell. An artificial intelligence-based machine learning model is developed to accurately predict and assess computationally generated data, identifying improved material use and process conditions. The investigation supports the assessment of providing high-quality, cleaned syngas to solid oxide cells for continuous r-SOC operation, furthering sustainable research in a safe, consistent manner.

## 2. Methodology

In a recent study [86], an experimentally validated CFD model based on Peksen et al. [65] was reconstructed and extended to predict the intricate syngas thermochemistry during the pre-reforming process. In this study, this model, with its enhanced capabilities, has

been used to generate quantitative data in a systematic manner, leveraging the Design of Experiments (DoE). This optimises the data generation process, thereby reducing the number of numerical simulations required to achieve the desired outcome. This approach provides multiple benefits, including the reduction of uncontrolled variables that can introduce errors, and the identification of key factors that influence the outcome of the assessment, thereby improving the overall performance of the data processing. To assess the optimal methane fuel utilisation, a supervised machine learning model was developed and trained, considering both individual parameter effects and interaction impacts of the examined variables. The approach has proven to be both cost-effective and sustainable, providing valuable research early in the process.

### 2.1. Numerical Modelling for AI Data Generation

Proper data preparation is a crucial aspect of AI-based modelling, involving the careful selection, cleaning, and preprocessing of data to ensure their high quality and suitability for training an artificial intelligence-based model. In this study, a numerically solved computational fluid dynamics (CFD) model was used to successfully generate data. The used pre-reformer component was modelled as a continuum using a pseudo-fluid phase, as depicted in Figure 1. For further details on the validation and utilisation of the model, readers are referred to Ref. [65].

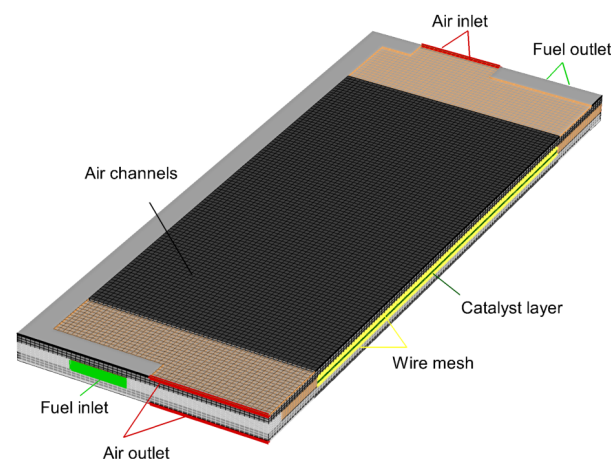


**Figure 1.** Used computational fluid dynamics model based on Ref. [65].

The present study considers a pre-reformer with two air flow plate layers that encompass the interior components, which are heated by the manifold regions. The catalyst layer is sandwiched between two wire mesh structures that facilitate the fuel flow. The pre-reformer has a symmetrical geometry and flow configuration along its centerline axis. This allows for a time efficient CFD analysis by simulating only half of the component. Syngas is used as the fuel medium in this study, and the focus is on determining the methane utilisation percentage, which is critical for delivering the desired fuel composition and amount for solid oxide cell operation. The simulation of the oxygen-containing syngas solves the tri-reforming (TR) reactions [42].

#### 2.1.1. Chemically Reacting Species Transport

The transport of chemically reacting species such as  $\text{CH}_4$ ,  $\text{CO}_2$ ,  $\text{H}_2\text{O}$ , and  $\text{O}_2$  is assumed to take place concurrently. The process involves the energy-efficient partial oxidation of methane, mitigating carbon formation. The numerical model takes into account the steam reforming and water-gas shift reactions, which are expressed as:





In this study, the methane reforming reaction (1) is considered to be kinetically slower and hence governs the methane conversion as the rate-limiting step. The reaction kinetics are dependent on the temperature and directly influence the conversion rate. Therefore, the operating temperature of the pre-reformer is a crucial parameter. The fuel used in this investigation contains a significant proportion of oxygen (5% to 10%). Thus, the chemical reaction characterising the partial oxidation of methane gas is included in the chemistry model, and it can be expressed as:



The calculations involving the oxygen-containing gas include  $\text{CH}_4$ ,  $\text{H}_2\text{O}$ , and  $\text{O}_2$  as reagents. The partial oxidation of methane is considered in the process, acting like an auto-thermal reforming reaction that generates clean syngas. However, since methane is consumed by this oxidation process, the methane that effectively takes part in the reforming reaction is reduced. As a result, the reforming rate depends on the  $\text{CH}_4$  amount that remains after it reacts with  $\text{O}_2$ .

The species transport model is based on single-phase flow field calculations. The local concentrations of species influence the flow field. Chemical reactions are considered to be homogeneous and take place at the catalyst layer. Turbulent fluctuations are not considered, and the reactions are driven kinetically by the Arrhenius kinetic expression, which is expressed as:

$$r_i = k_f \prod_{j=1}^{N_{sp}} |C_j|^{\eta'} - k_b \prod_{j=1}^{N_{sp}} |C_j|^{\eta''} \quad (4)$$

In this expression,  $N$  specifies the number of the chemical species in the reaction,  $C_j$  refers to the molar concentration of reactant and product species,  $\eta'$  denotes the forward rate exponent of each reactant and product species, and  $\eta''$  indicates the reverse proceeding backward reaction rate exponent.  $k_f$  and  $k_b$  express the forward and backward equilibrium constants, respectively. The rate constant shown as  $k$  for each reaction ( $r$ ) is calculated using equation:

$$k_r = A_r T^{\beta} e^{-E/RT} \quad (5)$$

" $A_r$ " is the pre-exponential factor, the temperature exponent is shown as " $\beta$ ", and the activation energy is " $E$ "; " $R$ " and " $T$ " represent the universal gas constant and temperature, respectively. Mass flow rates, operating temperatures, and species concentrations are specified for the fluid flow inlet regions. Each species is treated using the multi-component approach, which is based on Maxwell's equations. Homogeneous chemical reactions are assumed to occur at the catalyst layer, and they are driven by the Arrhenius kinetic expression.

### 2.1.2. Fluid Flow

The differential expression of the principle of conservation of mass is utilised at all points within the fluid domain to ensure that the mass balance is maintained. This equation expresses that, within a particular region, the rate of change of mass is equal to the net mass flux across the boundary of that region.

$$\frac{\partial \rho}{\partial t} + \nabla \cdot \rho \mathbf{U} = 0 \quad (6)$$

Using the product rule, momentum conservation is defined as:

$$\nabla \cdot (\rho \mathbf{u} \mathbf{U}) = \mathbf{U} \cdot \nabla (\rho \mathbf{u}) + \rho \mathbf{u} \cdot \nabla \mathbf{U}. \quad (7)$$

The pre-reformer component comprises materials and components that are porous in nature. To account for the momentum conservation in such media, the continuum theory of

porous media is applied. This is mathematically achieved by incorporating a momentum source term into the Navier–Stokes equations, as detailed in Ref. [87].

### 2.1.3. Energy

Conjugate heat transfer is an important factor in thermal energy exchange, and accurately estimating the temperature of the fluid within the flow field is crucial. To solve the thermal fluid flow problem, the energy equation must include this dependent variable. This relationship can be expressed as a vector:

$$\frac{\partial \rho h}{\partial t} = -\nabla \cdot (\rho h \mathbf{u}) - \nabla \cdot \mathbf{q} - (\boldsymbol{\tau} : \nabla \mathbf{u}) - p(\nabla \cdot \mathbf{u}) + S \quad (8)$$

where  $h$  is given as the enthalpy,  $t$  refers to the temperature,  $\mathbf{u}$  is the fluid velocity,  $\mathbf{q}$  expresses the heat conduction, and  $\boldsymbol{\tau}$  refers to the viscous part of the stress tensor.  $S$  comprises the source terms of the chemical reactions.

Due to the heat exchanging fluid flow, variations in density arise; these can have a significant impact on the overall flow behavior. These variations in density can be attributed to the pressure and temperature fluctuations; as such, these parameters must be interrelated to accurately describe the flow. The equation of state provides a means of coupling the pressure and specific internal energy ( $ie$ ) to describe the thermodynamic behavior of the system. This relationship is crucial for accurately predicting the behavior of the fluid within the flow field, especially in cases where temperature and pressure variations are significant and can be described as:

$$\begin{aligned} p &= p(\rho, T) \\ ie &= ie(\rho, T) \\ p &= \rho RT \\ ie &= CT \end{aligned} \quad (9)$$

where  $R$  is the ideal gas constant and  $C$  refers to the specific heat capacity. The total enthalpy resulting from species transport can be expressed as:

$$h = \nabla \cdot \left( \sum_j X_j \vec{h}_j \right) \quad (10)$$

$X_j$  is the species mass fraction shown as  $j$ . At the given reference temperature, the expression for the production of sensible enthalpy by the species  $j$  is:

$$h_j = \int_{T_{refj}}^T c_{pjd} T + h_j^0(T_{refj}) \quad (11)$$

In Equation (8), the chemically reacting species transport term is presented as a source term denoted by the symbol  $S$ . This term represents the rate of change of species concentrations due to chemical reactions. This source term is crucial for accurately modeling the chemical reactions within the system and predicting the behavior of the fluid flow.

It can be expressed as the source term for chemical reactions:

$$S := -\sum_j \frac{h_j^0}{M_j} R_j \quad (12)$$

With  $R_j$  as the volumetric rate of creation of the species,  
The heat transfer of the solid regions is described as:

$$\frac{\partial \rho h}{\partial t} + \nabla \cdot (\rho h \mathbf{u}) = \nabla \cdot (k \nabla T) + S \quad (13)$$

The convective term on the left-hand side describes the heat transfer between the solid walls and the fluid. Where  $h$  will be calculated from:

$$h_j = \int_{T_{refj}}^T c_{pj} dT + h_j^0 \quad (14)$$

## 2.2. Computational Assessment

The current investigation employs two different gas compositions: one with high oxygen with low methane content, and the other containing moderate oxygen gas with a high methane concentration. In a typical system operation, the cathode outlet gas from the SOC stack is linked to the air intake of the external pre-reformer component, which helps to determine the air inlet conditions of the pre-reformer, as shown in Figure 2, proposed by Blum et al. [88]. Thus, the current research considers a data set of pre-heated air of 750 °C and 30 kg/h that feeds the pre-reformer with an air input temperature of 724 °C. The fuel inlet temperature is set at 155 °C. These specific values were chosen based on previous studies and are typical operating conditions for this type of system configuration. It is important to note that variations in operating conditions can significantly affect the performance of the system. Therefore, systematic analyses will be performed to evaluate the robustness of the results.

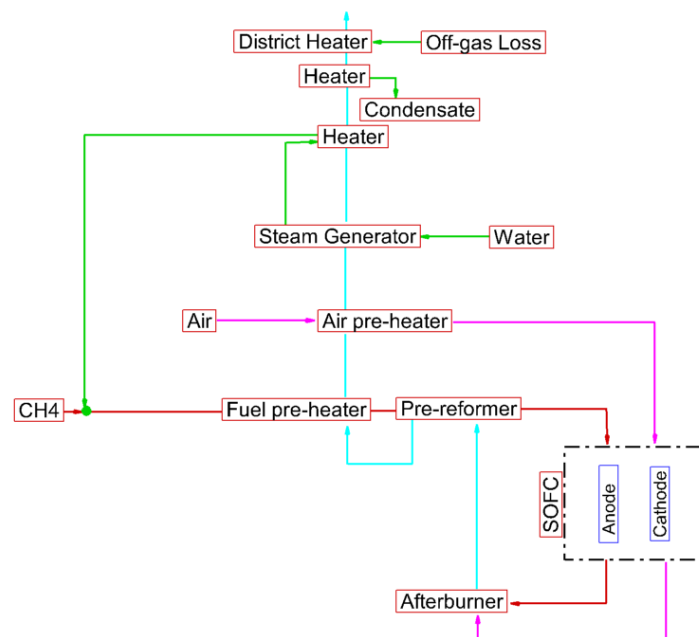


**Figure 2.** Sample SOFC concept with external reforming based on Ref. [88].

Methane fuel utilisation is an important performance metric in the pre-reforming process; it is used to convert hydrocarbon fuels into hydrogen gas. The amount of methane that enters the pre-reformer and the amount that exits unconverted represents the amount of methane that was converted to hydrogen gas. Simply, it represents the fraction of the fuel that is converted to hydrogen gas during the reforming process. Understanding the fuel utilisation of the cleaned syngas when using a pre-reformer is an important factor in optimising the fuel cell stack inlet conditions. By carefully monitoring the reformed fuel outlet, it is possible to gain an indication of the amount of methane that can be used in SOC operation for cooling purposes. This can help ensure the most efficient use of the fuel cell stack. In order to use dataset for the development and further deployment of an artificial intelligence model, the effects of several operating parameters are systematically assessed. This will reduce the prediction time and the need for additional CFD analyses. The conversion rate of pre-reformed methane in this current study will be analysed in

relation to its dependence on five parameters, each of which has three distinct degrees. In this case, the nonlinear interactions of the variables are considered.

A three-factor level approach will express the lowest, median, and maximum levels of the variables. The stated process parameters, and the quantitative prediction of the methane utilisation percentage (in this context, it is the conversion as the mass flow rate is constant), is the outcome. An efficient Design of Experiment (DoE) plan [89] is used and the investigated variables are illustrated in Table 1.

**Table 1.** Investigated variables used for the Design of Experiment (DoE) assessment.

Factor Level	−1	0	1
Fuel_mass flow rate [kg/s]	A	B	C
Air_mass flow rate [kg/s]	A	B	C
Air temperature [°C]	640	700	725
Fuel oxygen content [%]	0	5	10
Catalyst porosity [-]	0.2	0.35	0.50

The catalyst layer's porosity corresponds to the void fraction of the substrate. Three different gas compositions are investigated, with oxygen concentrations of 0%, 5%, and 10%, denoted as A, B, and C, respectively, as given in Table 1. The gas mass flow rates are also included, as they affect the quantity of energy introduced to the component. The fuel input temperature is set at 155 degrees Celsius in all cases, and the porosities of the catalyst materials are chosen based on commonly observed values. A total of 48 instances were computed to illustrate the various combinations of factor levels, providing the necessary output data for statistical analysis.

### 2.3. Artificial Intelligence-Based Machine Learning (ML) Modelling

In this study, quantitative data has been generated using an experimentally validated CFD model to develop and train a machine learning model based on supervised learning. Supervised learning is a machine learning field in which large data sets are provided to develop a mathematical model that can reliably predict values of previously unknown data. The first step in this process is the collection and preparation of numerical data. This involves identifying and correcting any data errors or inconsistencies, such as missing values, incorrect data types, or outliers. Data processing ensures the accuracy and reliability of the data.

The data may need to be transformed to conform to the model's specifications. This could include scaling the data to a common range, normalising it, or converting categorical variables into numerical values. The most relevant features are selected to train the model to reduce its complexity and improve its performance. After processing, transforming, and selecting features, the data is separated into two or three distinct sets: a training set, a validation set, and a test set. The validation part is used to tune the model's hyperparameters, and the test set is used to evaluate the model's performance.

Data augmentation is used to create new training data for the model by applying transformations to existing data, which helps to improve the model's robustness and reduce overfitting.

The independent variables are used to describe the parameters, while the dependent variable or response variable is known as the target variable of interest. The CFD model generated numerical data, which were divided into two data sets for training and evaluating the model. Since steady-state analyses were performed, the nature of the data was not categorical or a function of time. As the collected data were numerical and continuous, a regression-type problem architecture was used instead of classification or time series. The supervised learning process was used to establish a relationship between the variables and

methane fuel utilisation. An algorithm was used to analyse the patterns in the data that enables the generation of new data.

Figure 3 depicts the procedure utilised in the present investigations.

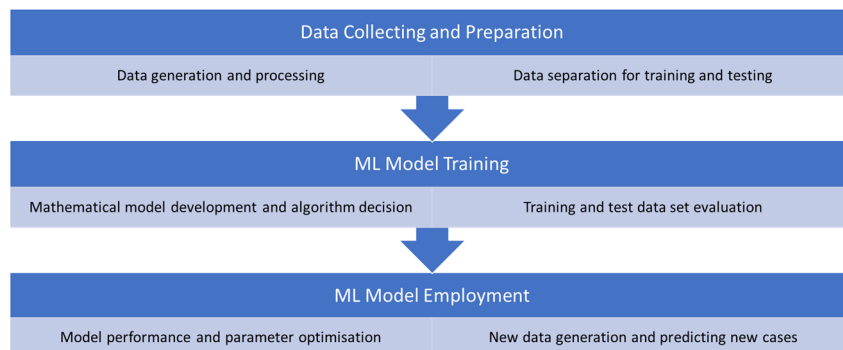


**Figure 3.** Flow chart of the machine learning (ML) model development and implementation.

The response variable is the methane fuel utilisation, which is a number; therefore, the problem type can be justified as a regression type. In this way, the model is trained by assigning labels to the data to enable the model to learn from it. The data labelling involves assigning a continuous numerical value to each data point. As the goal is to predict methane fuel utilisation, the label represents the percentage. The quality of the labelled data can have a significant impact on the accuracy of the model. Therefore, high-quality data have been used that are free from errors and inconsistencies. To avoid the issue with the so-called overfitting, the validation set was used. Overfitting occurs when the model is trained too closely to the labelled data, leading to poor performance on new data. To mitigate this, the model's parameters are carefully assessed. It refers to settings such as regularisation strength or learning rate, iteration number, step size, and batch size controlling each iteration of the training process. A similar process is performed in CFD analysis for reaching convergence. Overall, artificial intelligence-based modelling is anticipated to accelerate the assessment based on the 3D pre-reformer behaviour, and the improvement potential has been pursued using the data provided by the CFD calculations.

### 2.3.1. Model Development

Building upon the findings of Section 2.3, the nonlinear relationship between the fuel utilisation percentage and the pertinent parameters will be established. Quadratic and cubic terms are considered in the model. A multi-regression modelling approach ensures that categorical variables, such as gas composition, can be used with the specified factor levels and values.

### 2.3.2. Model Training Based on Machine Learning (ML)

To evaluate the model's feasibility, an assessment of outliers and model quality is conducted for different regression models. For the learning-training procedure, the initial set of numerically calculated data is used to train the model, while the test data are used then to evaluate the level of model accuracy. Model regression coefficients can be learned and trained using the proposed data set. A k-fold cross-validation divides the data into sections for training purposes. This is performed multiple times using different partitions of the data followed by averaging the results to obtain an estimate of the model's performance on unseen data. The data have been divided into ten subsets of roughly equal size. The model is trained on nine subsets and evaluated on the remaining subset. This procedure is repeated ten times, with each subset serving as the validation set once. The results are averaged to obtain an estimate of the model's performance. The fold number determines the computational effort and evaluates the optimisation potential of the model. The procedure facilitates model comparison and selection. Details of the procedure are given in Ref. [85].

### 2.3.3. ML Model Validation

Three different regression models are benchmarked to assess the methane fuel utilisation. The objective was to evaluate the model's ability to generalise to new data and identify any issues. The root mean squared error (RMSE) metric is used to interpret the model accuracy. This is the square root of the mean squared error (MSE) and provides a measure of the average absolute difference between the predicted and actual values of the target variable. A lower RMSE indicates better performance. The MSE measures the average squared difference between the predicted and actual values of the target variable. The common R-squared ( $R^2$ ) is also used. An  $R^2$  of 1 indicates an excellent prediction level, while an  $R^2$  of 0 indicates that the model does not explain any of the variance in the target variable. A confidence interval of 95% was utilised to estimate the true population parameters. Using this interval is aimed at capturing the range within which the population mean is likely to fall within 95% confidence. This approach provides a level of precision and reliability in the estimations, allowing for robust conclusions and informed decision making. The stochastic Optimizable Gaussian Progress Regression (GPR) model is the first model trained. This type is beneficial when data sets with a normal distribution are of concern. A support vector machine (SVM) model of cubic form is also trained in case data classes are formed. The third variant to be considered was a linear regression model. The model results are compared to a more complex multiple regression model. Figure 4 illustrates the results of the predictions compared to the true response results of the observed  $\text{CH}_4$  utilisation%.

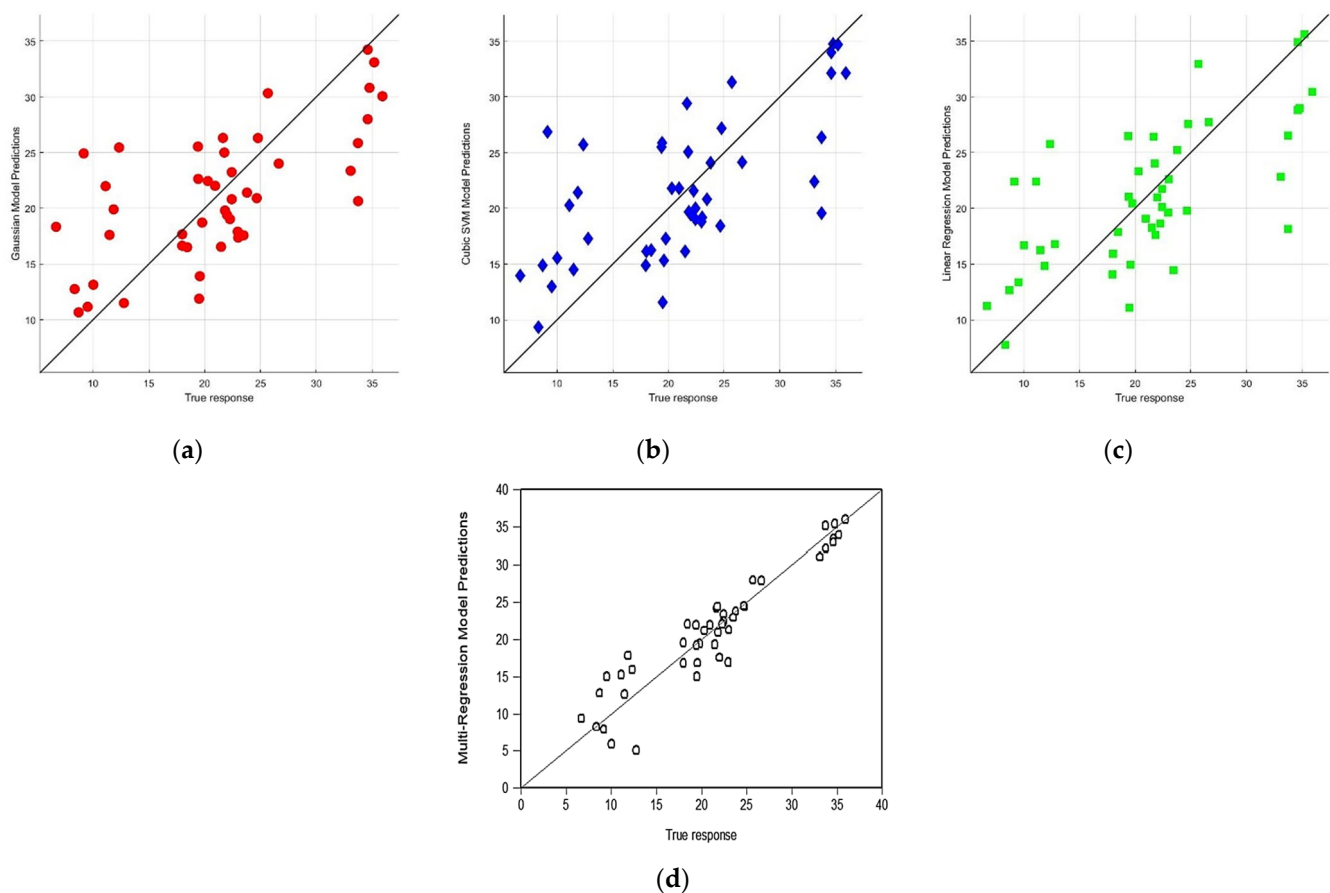


**Figure 4.** Model development and comparison of different regression models: GPR (a); SVM (b), linear-regression (c), multi-regression model (d).

Although the residual data are spread across the theoretical normal distribution line, outliers were evident in both the Optimizable Gaussian Progress Regression (GPR) model,

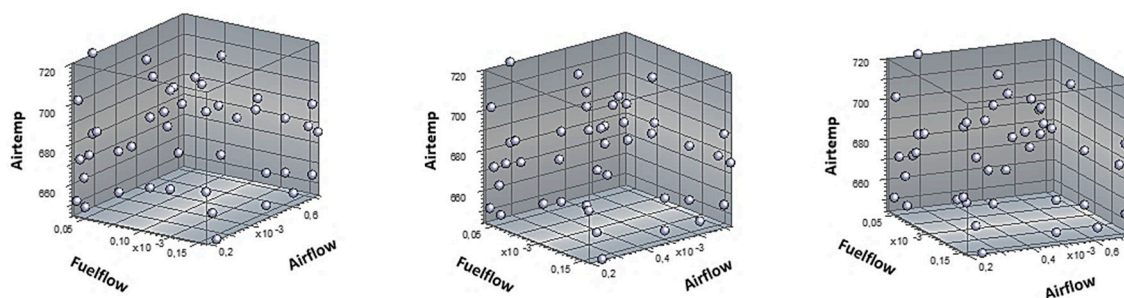
depicted in Figure 4a, and the support vector machine (SVM) model, depicted in Figure 4b. The assessed linear-regression model depicted in Figure 4c showed similar behaviour. The residuals of the multi-regression approach are closer to the straight line when compared to the other three models (Figure 4d). These models each show outliers. The use of a robust linear regression algorithm that can be used to handle outliers did not result in an improvement. Moreover, the validation values of the multi-regression model outperformed the remaining models used as a benchmark in Figure 4d.

Table 2 shows the data for the quality evaluation.

**Table 2.** Quality evaluation of the used models considering  $R^2$ , RMSE values.

	GPR	SVM	Linear-Regression	Multi-Regression
RMSE	5.50	6.08	5.88	4.096
R-Squared	0.57	0.48	0.50	0.93

Based on the conducted analysis, the decision was made to implement a more complex cubic multi-regression machine learning model. This choice was made as the quality of the remaining models remained unsatisfactory, despite using methods such as principal component analysis (PCA) or hyperparameter optimisation. The data points were meticulously assessed to ensure that the entire range of values for each factor was accounted for. If certain regions of the cube had no points, it could indicate that the design was incomplete and that certain factor combinations were not explored. Figure 5 depicts the distribution of the data points in the design space using a three-dimensional cube plot.



**Figure 5.** Three-dimensional cube plot to assess the data range: All three different view angles depict a uniform data distribution.

The design points show a satisfactory evenly distributed behaviour across the cube. Considering the three-factor levels and the complexity of the process, this indicates that the regions of interest are neither over- nor under-represented. Moreover, the points are not clustered in certain regions, suggesting that the data cover several regions and shows uniformity. The trained model has been used to assess the individual process variables to predict a practicable methane fuel utilisation of 20%. It has been targeted to use the same substrate and syngas combination, comprising 5% of oxygen, and to assess the possible fuel amount and air temperature. Figure 6 shows the results.

By adjusting the air temperature value, it is possible to achieve the desired 20%  $\text{CH}_4$  fuel utilisation under the current settings. The nonlinear cubic behaviour of the air temperature curve is apparent, as it shows a more energy-efficient output on the lower side of 666 °C and on the higher side of 709 °C, both resulting in a 20% fuel utilisation. Moreover, the nonlinear nature of the variable suggests that it has the potential to increase the methane utilisation beyond 20% if adjusted independently.

In order to evaluate the performance of the trained model using fuel flow rate, catalyst substrate porosity, and oxygen% content, Figure 7 presents the assessment results.

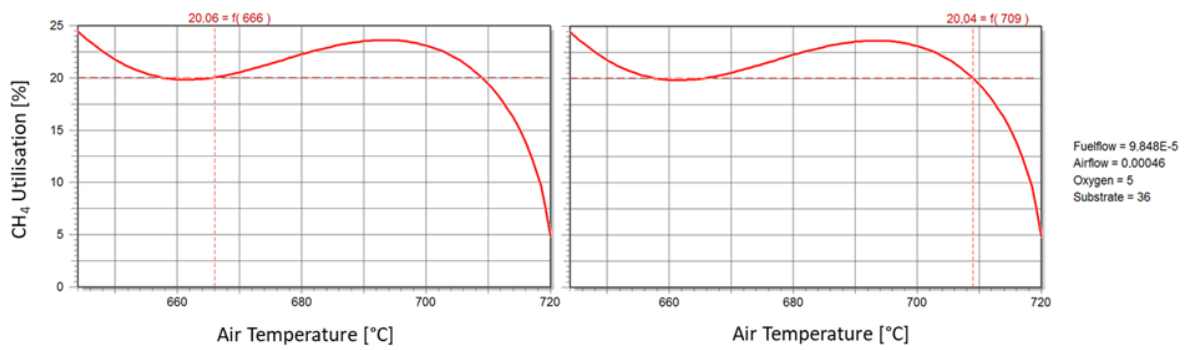


Figure 6. Trained model employment: assessment of the CH<sub>4</sub> utilisation as a function of temperature.

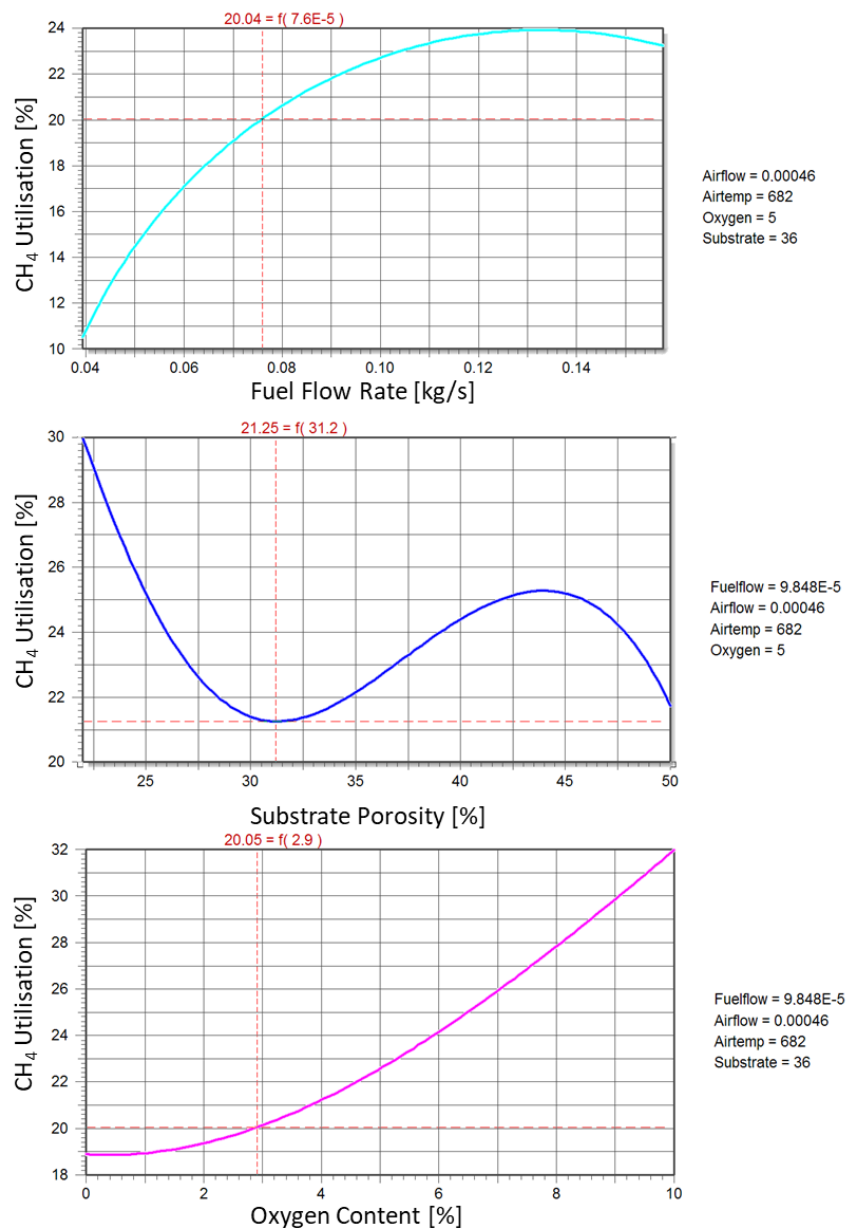
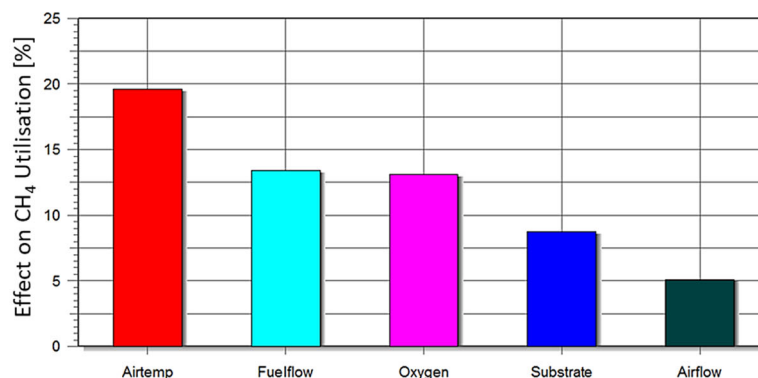


Figure 7. Trained model employment: assessment of the CH<sub>4</sub> utilisation as a function fuel flow rate, substrate porosity, and oxygen content.

The trained model was evaluated individually for each parameter. The results suggest that a methane fuel utilisation rate of 20% can be achieved by using a fuel flow rate of

$7.6 \times 10^{-4}$  kg/s or by increasing the substrate porosity. The nonlinear cubic behaviour of the substrate porosity indicates that a porosity of approximately 31% is optimal for achieving the desired methane utilisation rate. Additionally, the quadratic behaviour of the oxygen concentration shows that an increase in oxygen content leads to an increase in methane utilisation percentage due to the increased partial oxidation reaction. Therefore, a lower oxygen content of around 3% is recommended for achieving the desired 20% methane utilisation rate. The complex mathematical relationship between the three-level factors and methane fuel utilisation was analysed to determine the main factors affecting  $\text{CH}_4$ . Figure 8 depicts the analysis results of the main factors affecting the  $\text{CH}_4$  fuel utilisation rate.



**Figure 8.** Effect analysis: Main parameters affecting the  $\text{CH}_4$  utilisation.

The findings of the study demonstrate that  $\text{CH}_4$  utilisation is highly sensitive to air temperature, as indicated by the results presented in Figure 6. The complex nature of the temperature's effect on the reactions is represented by its strong nonlinearity under fixed remaining parameters. The temperature-dependent nature of the chemical reactions and the energy required to initiate them necessitates a certain level of temperature for the reactions to occur. As a result, temperature received the highest weighting, followed by fuel amount, as it is also a limiting factor. Insufficient fuel for conversion would lead to utilisation failure. The exothermic impact of the oxygen-driven partial oxidation reaction contributes significantly to providing the necessary thermal energy for utilisation and leads to a substantial increase in fuel conversion, as depicted in Figure 6. On the other hand, the effects of substrate porosity and air flow, when used as a sole design tool, were found to be less significant than the first three factors.

### 3. Optimisation Using the Machine Learning Model

In this section, the predictive economic tool for accelerated process and material optimisation was demonstrated using the capability of the trained model. Under virtual operating conditions, the methane fuel utilisation rate of the reformer was simulated to mitigate prohibitive measurements. In situations where there may be a concern for detailed distributions of temperature, species concentrations, or pressure, the rapid predictions of the machine learning model also allow for screening purposes. Hence, the model can be deployed either independently or in conjunction with conventional methods.

#### 3.1. Assessment for Potential Material Optimisation

Fluid flow, heat transfer, and chemical reaction conditions are essential to gain a deeper understanding of the process interactions while reforming oxygen-containing syngas. The interactions and nonlinear behaviour of these factors play a critical role in SOC systems that use syngas. These factors influence the inlet gas composition of the fuel cell stack. In addition, by pre-reforming a portion of the fuel gas, the oxygen can be utilised while ensuring that no oxygen is later released into the fuel cell stack. Machine learning predictions will provide invaluable information to enhance the control of species and methane fuel utilisation during the process. Thus, controlled quality syngas can be generated by specify-

ing the methane fuel species mass fractions of the reformed syngas in SOC operation. To achieve a controlled methane fuel utilisation of ~20% under the applied process conditions, a nonlinear analysis of the factors has been conducted to comprehend the interactions among the parameters during the pre-reforming process.

To evaluate the possibility of reducing the solid material amount in the catalyst and enhancement of resource sustainability, the level of porosity of the substrate materials used during the pre-reforming process is crucial. The substrate’s porosity affects the access of the reactants to the active sites. Low substrate porosity can lead to poor species transport, reduced access of the reactants to the catalyst, lower reaction rates, and reduced thermos chemical efficiency. For this purpose, two distinct cases have been investigated under the same process conditions. The outcomes of the analysis are illustrated in Figure 9.

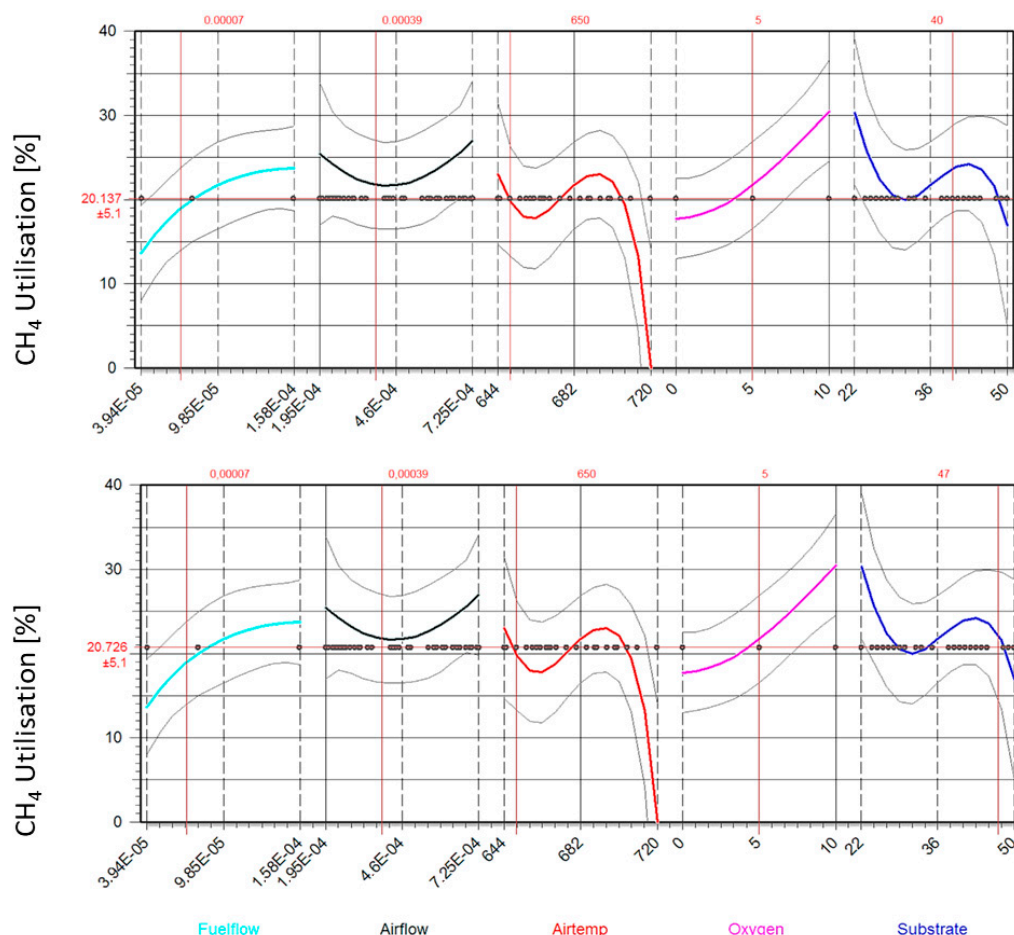


Figure 9. Assessment of the material reduction potential by keeping target CH<sub>4</sub> utilisation.

Using the developed ML model, it was possible to determine the substrate porosity values required to achieve a methane fuel utilisation rate of 20%. An optimally selected porous catalyst is environmentally friendly because it uses less material, and it may also facilitate enhanced chemical reaction performance with the targeted fuel utilisation output. The nonlinear behaviour of the substrate curve indicates the possibility of reducing the amount of catalyst material while still achieving 20% CH<sub>4</sub> utilisation. The results reveal that the desired utilisation level can be achieved in two ways, one at the low end of the factor range and the other at the high end.

Approaching a void fraction of 40%, compared to a less dense open structure of 47%, showed to be feasible to retain the desired methane fuel utilisation. The results reveal that it is possible to use a substrate with a reduced solid fraction of around 11.7%. This would enable less material as well reduce catalyst costs that may contribute to an overall cost

reduction in the integrated technology concepts. The results were compared to the detailed 3D CFD-calculated predictions for verification purposes. The comparison of the results is listed in Table 3.

**Table 3.** Comparison of machine learning model predictions vs. 3D CFD analyses.

	Fuel [kg/s]	Air [kg/s]	Air [°C]	O <sub>2</sub> [%]	Catalyst	% ML	% CFD	% Error
Case 1	$7.0 \times 10^{-5}$	$3.9 \times 10^{-4}$	650	5	40	20.14	20.52	−1.76
Case 2	$7.0 \times 10^{-5}$	$3.9 \times 10^{-4}$	650	5	47	20.73	20.48	1.22

The calculated methane fuel utilisation% values are in excellent agreement with the CFD predictions. The model is approved to be a predictive optimisation instrument where the sustainable use of materials with specific methane utilisation outputs is targeted.

### 3.2. Assessment for Potential Process Optimisation

The optimisation of methane fuel utilisation in the reforming process presents a challenge as the thermochemical processes are very complex. The model was employed to determine the required amount of fuel for specified methane utilisation conditions. Process optimisation efforts offer several advantages, including reducing the amount of trial and error necessary to optimise the process, saving time and resources, and predicting the required optimal parameters for fuel utilisation, enabling rapid adjustments if necessary. Moreover, it improves the overall efficiency of the process, resulting in lower costs and fewer emissions. Given the use of an oxygen-containing medium in the current process, it is a safe method.

The controlled operation of the pre-reforming process with specific methane fuel utilisation is essential to ensure the success of SOC operation. It directly influences the efficiency and performance of the SOC. The arbitrary release of methane fuel concentration into the SOC can cause deposition issues on the anode, leading to a performance reduction and eventual failure of the components. On the other hand, incomplete conversion can occur if the methane concentration is too low, resulting in a decrease in power output. Monitoring and maintaining the methane concentration at the desired optimal level is crucial to ensure the efficient and reliable operation of solid oxide cells, resulting in cost savings and reduced environmental impact. Figure 10 displays the prediction results of the process possibilities to achieve fuel utilisation percentages of 20%, 25%, and 30% using a substrate material with a porosity of 44%, depicting a range closer to the higher parameter level.

The plot of the predicted curves illustrates the complex nonlinear behaviour of the investigated parameters. The slope of each variable indicates the level of its effect that can be adjusted. Based on the relationships, it was possible to assess and determine process conditions with the desired methane fuel utilisation%. The current analyses considered processes that maintained stable temperature, constant oxygen content, and the same substrate. The target was to use the fuel and air mass flow rates in an economical manner to achieve a methane fuel utilisation of 20%, 25%, and 30%. Increasing the fuel flow rate can result in higher pre-reforming methane fuel utilisation, which means that more methane will be converted into hydrogen and carbon monoxide.

However, if the air flow rate remains insufficient, the oxygen supply may not be sufficient for the increased amount of methane, leading to incomplete conversion and the production of carbon dioxide and unreacted methane.

Reducing the fuel flow rate can decrease the fuel utilisation percentage, resulting in lower hydrogen production. However, if the airflow rate is systematically adjusted, the process can remain balanced, resulting in the desired output. The present research results indicate that the fuel flow behaviour influences methane fuel utilisation percentage levels non-linearly, approaching higher levels from a nearly linear state. This behaviour could indicate an increased mass flow rate utilization.

The optimal configuration of model parameters is important because if more gas is available for a chemical reaction-induced heat transfer, the more likely it will be that methane concentration can remain as excess gas at the outlet region, resulting in reduced methane utilisation. The air flow rate shows an exponential drop approaching low-level values to the mid-range level, and it increases with similar behaviour, building a parabolic curve. The fuel mass flow rate requires an increase of 58% to increase the baseline 20% methane fuel utilisation to 25%. Similarly, the methane utilisation percentage could be increased to 30% by increasing the fuel flow rate by 33% while allowing the air flow rate to decrease by 28%. However, solely increasing the mass flow rates was insufficient.

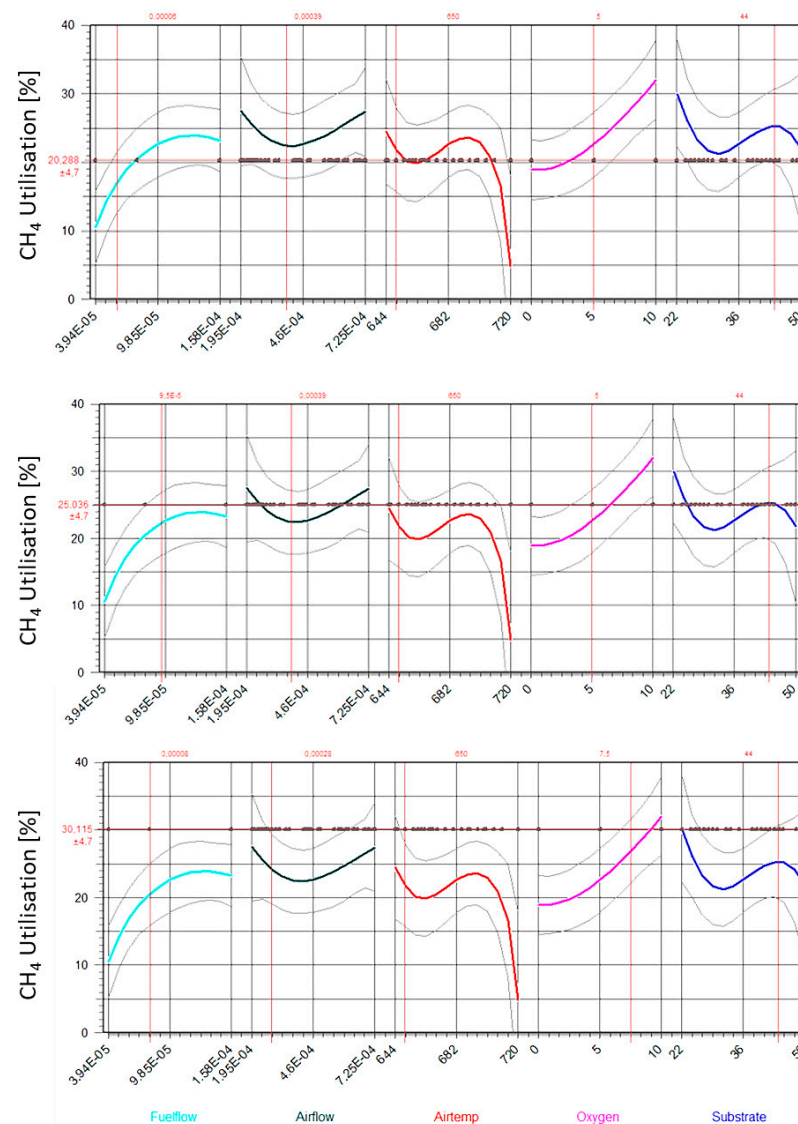


**Figure 10.** Assessment of an improved process potential by targeting specific CH<sub>4</sub> utilisation%.

In a recent study, a cost-effective approach was shown to maintain an air flow rate at a medium temperature set at 650 °C [86]. Thus, it was assessed whether it was possible to maintain the conditions and the catalyst porosity at a constant level and try to achieve the desired methane utilisation targets with mass flow rate optimisation. It should be noted that, when compared to the 20% methane utilisation case, an economic option could still be achieved as both the used air and fuel mass flow rates could be reduced by increasing the oxygen content to 7.5% instead of the targeted 5%. This can be attributed to the close interaction between the air mass flow rate and the increased oxygen level, as the chemical

reactions in the process are a function of oxygen concentration. This contributes to an energy-efficient and sustainable solution in the utilisation of process gases.

#### 4. Conclusions

This article investigates the optimal conditions for pre-forming during SOC-ready syngas preparation. Using a 3D CFD pre-reformer model, the integrated Tri-reforming (TR) chemical reactions and thermofluid flow of syngas-containing fluids have been systematically solved to predict methane fuel utilisation. The validated model has been used to efficiently generate input for the development and training of an accelerated machine learning model. Process and material parameters, including flow rates, air temperature, different levels of oxygen-containing gas compositions, and various catalyst substrate configurations, have been considered. The AI-based model results indicate that an 11% reduction in substrate material could be achieved by maintaining the desired parameters at the targeted 20% methane fuel utilisation. This could be attributed to the nonlinear effect of the substrate on methane fuel utilisation. When the predicted data and the result of the 3D CFD analyses were compared, an excellent agreement was observed. Systematic process optimisation efforts reveal that it was possible to gain 5% in methane fuel utilisation by maintaining a moderate air temperature of 650 °C under constant air flow and gas composition. The fuel mass flow rate required an increase of 58%. Similarly, the methane utilisation% could be increased to 30% by increasing the fuel flow rate by 33% while allowing the air flow rate to decrease by 28%. A compromise has been given to increase the fuel oxygen content as it was not possible to reach the high utilisation% otherwise. The accelerated AI-based model demonstrated outstanding performance in promoting sustainable research. In addition, it enhanced the understanding of controlled quality syngas preparation for upcoming continuous SOC operation with reduced operation risks. The approach has great potential for future research on accelerated data supply especially when additional variables are considered and complex machine learning models are trained on different platforms.

**Funding:** My gratitude goes to the Federal Ministry of Education and Research (BMWF), which is funding this project with the code 01DD21005.

**Data Availability Statement:** Data sharing is not applicable to this article as research is on-going.

**Acknowledgments:** The authors gratefully acknowledge the International Future Laboratory at the Technical University of Munich (TUM) for the collaboration throughout of the REDEFINE H2 project.

**Conflicts of Interest:** The authors declare no conflict of interest.

#### References

1. Ivers-Tiffée, E.; Weber, A.; Herbstritt, D. Materials and technologies for SOFC-components. *J. Eur. Ceram. Soc.* **2001**, *21*, 1805–1811. [[CrossRef](#)]
2. Delette, G.; Laurencin, J.; Usseglio-Viretta, F.; Villanova, J.; Bleuët, P.; Lay-Grindler, E.; Le Bihan, T. Thermo-elastic properties of SOFC/SOEC electrode materials determined from three-dimensional microstructural reconstructions. *Int. J. Hydrogen Energy* **2013**, *38*, 12379–12391. [[CrossRef](#)]
3. Cui, D.; Yang, C.; Huang, K.; Chen, F. Effects of testing configurations and cell geometries on the performance of a SOFC: A modeling approach. *Int. J. Hydrogen Energy* **2010**, *35*, 10495–10504. [[CrossRef](#)]
4. Froitzheim, J.; Meier, G.; Niewolak, L.; Ennis, P.; Hattendorf, H.; Singheiser, L.; Quadackers, W. Development of high strength ferritic steel for interconnect application in SOFCs. *J. Power Sources* **2008**, *178*, 163–173. [[CrossRef](#)]
5. Peksen, M. 3D CFD/FEM analysis of thermomechanical long-term behaviour in SOFCs: Furnace operation with different fuel gases. *Int. J. Hydrogen Energy* **2015**, *40*, 12362–12369. [[CrossRef](#)]
6. Rasmussen, J.F.B.; Hendriksen, P.V.; Hagen, A. Study of Internal and External Leaks in Tests of Anode-Supported SOFCs. *Fuel Cells* **2008**, *8*, 385–393. [[CrossRef](#)]
7. Dokiya, M. SOFC system and technology. *Solid State Ionics* **2002**, *152–153*, 383–392. [[CrossRef](#)]
8. Nguyen, X.-V.; Chang, C.-T.; Jung, G.-B.; Chan, S.-H.; Lee, W.-T.; Chang, S.-W.; Kao, I.-C. Study of sealants for SOFC. *Int. J. Hydrogen Energy* **2016**, *41*, 21812–21819. [[CrossRef](#)]
9. Tietz, F. Thermal expansion of SOFC materials. *Ionics* **1999**, *5*, 129–139. [[CrossRef](#)]
10. George, R.A. Status of tubular SOFC field unit demonstrations. *J. Power Sources* **2000**, *86*, 134–139. [[CrossRef](#)]
11. Föger, K.; Love, J. Fifteen years of SOFC development in Australia. *Solid State Ionics* **2004**, *174*, 119–126. [[CrossRef](#)]

12. Blum, L.; Batfalsky, P.; Fang, Q.; de Haart, L.G.J.; Malzbender, J.; Margaritis, N.; Menzler, N.H.; Peters, R. SOFC Stack and System Development at Forschungszentrum Jülich. *J. Electrochem. Soc.* **2015**, *162*, F1199–F1205. [[CrossRef](#)]
13. Peksen, M.; Al-Masri, A.; Peters, R.; Blum, L.; Stolten, D. Recent Developments of 3D Coupled Multiphysics SOFC Modelling at Forschungszentrum Jülich. *ECS Trans.* **2013**, *57*, 2537–2541. [[CrossRef](#)]
14. Huang, C.; Shy, S.; Lee, C. On flow uniformity in various interconnects and its influence to cell performance of planar SOFC. *J. Power Sources* **2008**, *183*, 205–213. [[CrossRef](#)]
15. Peksen, M. A coupled 3D thermofluid–thermomechanical analysis of a planar type production scale SOFC stack. *Int. J. Hydrogen Energy* **2011**, *36*, 11914–11928. [[CrossRef](#)]
16. Greco, F.; Nakajo, A.; Wuillemin, Z.; Van Herle, J. Thermo-Mechanical Reliability of SOFC Stacks during Combined Long-Term Operation and Thermal Cycling. *ECS Trans.* **2015**, *68*, 1921–1931. [[CrossRef](#)]
17. Fang, Q.; Blum, L.; Batfalsky, P.; Menzler, N.H.; Packbier, U.; Stolten, D. Durability test and degradation behavior of a 2.5 kW SOFC stack with internal reforming of LNG. *Int. J. Hydrogen Energy* **2013**, *38*, 16344–16353. [[CrossRef](#)]
18. Peksen, M.; Meric, D.; Al-Masri, A.; Stolten, D. A 3D multiphysics model and its experimental validation for predicting the mixing and combustion characteristics of an afterburner. *Int. J. Hydrogen Energy* **2015**, *40*, 9462–9472. [[CrossRef](#)]
19. Peksen, M.; Peters, R.; Blum, L.; Stolten, D. 3D coupled CFD/FEM modelling and experimental validation of a planar type air pre-heater used in SOFC technology. *Int. J. Hydrogen Energy* **2011**, *36*, 6851–6861. [[CrossRef](#)]
20. Douvartzides, S.; Coutelieris, F.; Demin, A.; Tsiakaras, P. Electricity from ethanol fed SOFCs: The expectations for sustainable development and technological benefits. *Int. J. Hydrogen Energy* **2004**, *29*, 375–379. [[CrossRef](#)]
21. Hafsia, A.; Bariza, Z.; Djamel, H.; Hocine, B.M.; Andreadis, G.M.; Soumia, A. SOFC fuel cell heat production: Analysis. *Energy Procedia* **2011**, *6*, 643–650. [[CrossRef](#)]
22. Föger, K.; Godfrey, B.; Pham, T. Development of 25 kW SOFC system. *Fuel Cells Bull.* **1999**, *2*, 9–11. [[CrossRef](#)]
23. Farhad, S.; Hamdullahpur, F.; Yoo, Y. Performance evaluation of different configurations of biogas-fuelled SOFC micro-CHP systems for residential applications. *Int. J. Hydrogen Energy* **2010**, *35*, 3758–3768. [[CrossRef](#)]
24. Peksen, M. Safe heating-up of a full scale SOFC system using 3D multiphysics modelling optimisation. *Int. J. Hydrogen Energy* **2018**, *43*, 354–362. [[CrossRef](#)]
25. Yi, Y.; Rao, A.D.; Brouwer, J.; Samuelsen, G.S. Fuel flexibility study of an integrated 25kW SOFC reformer system. *J. Power Sources* **2005**, *144*, 67–76. [[CrossRef](#)]
26. Lee, K.H.; Strand, R.K. SOFC cogeneration system for building applications, part 2: System configuration and operating condition design. *Renew. Energy* **2009**, *34*, 2839–2846. [[CrossRef](#)]
27. Fang, Q.; Blum, L.; Peters, R.; Peksen, M.; Batfalsky, P.; Stolten, D. SOFC stack performance under high fuel utilization. *Int. J. Hydrogen Energy* **2015**, *40*, 1128–1136. [[CrossRef](#)]
28. Blum, L.; Packbier, U.; Vinke, I.C.; de Haart, L.G.J. Long-Term Testing of SOFC Stacks at Forschungszentrum Jülich. *Fuel Cells* **2012**, *13*, 646–653. [[CrossRef](#)]
29. Rechberger, J.; Kaupert, A.; Hagerskans, J.; Blum, L. Demonstration of the First European SOFC APU on a Heavy Duty Truck. *Transp. Res. Procedia* **2016**, *14*, 3676–3685. [[CrossRef](#)]
30. Ho, T.X.; Kosinski, P.; Hoffmann, A.C.; Vik, A. Numerical analysis of a planar anode-supported SOFC with composite electrodes. *Int. J. Hydrogen Energy* **2009**, *34*, 3488–3499. [[CrossRef](#)]
31. Peksen, M.; Peters, R.; Blum, L.; Stolten, D. Hierarchical 3D multiphysics modelling in the design and optimisation of SOFC system components. *Int. J. Hydrogen Energy* **2011**, *36*, 4400–4408. [[CrossRef](#)]
32. Riensche, E.; Achenbach, E.; Froning, D.; Haines, M.; Heidug, W.; Lokurlu, A.; von Andrian, S. Clean combined-cycle SOFC power plant—Cell modelling and process analysis. *J. Power Sources* **2000**, *86*, 404–410. [[CrossRef](#)]
33. Peksen, M.; Al-Masri, A.; Peters, R.; Blum, L.; Stolten, D. 3D Multiphysics Modelling and Design Optimisation of a Complete SOFC System Operating in Jülich. *ECS Trans.* **2014**, *64*, 155–159. [[CrossRef](#)]
34. Peksen, M.; Al-Masri, A.; Peters, R.; Blum, L.; Stolten, D. Recent Developments in 3D Multiphysics Modelling of Whole Fuel Cell Systems for Assisting Commercialisation and Improved Reliability. *ECS Trans.* **2017**, *75*, 15–22. [[CrossRef](#)]
35. Peksen, M.; Al-Masri, A.; Blum, L.; Stolten, D. 3D Coupled Thermofluid-Thermomechanical Modelling and Experimental Validation of a Whole Solid Oxide Fuel Cell System. *ECS Trans.* **2013**, *50*, 139–142. [[CrossRef](#)]
36. Yang, C.; Jing, X.; Li, P.; Kan, A.; Wu, Y.; Ye, W.; Yuan, J. Performance analysis of mesoscale reactions in fuel electrode and effect on dynamic multiphysics processes in rSOFC with syngas. *Int. J. Hydrogen Energy* **2021**, *46*, 9523–9540. [[CrossRef](#)]
37. Shen, M.; Ai, F.; Ma, H.; Xu, H.; Zhang, Y. Progress and prospects of reversible solid oxide fuel cell materials. *iScience* **2021**, *24*, 103464. [[CrossRef](#)]
38. Yang, C.; Jing, X.; Miao, H.; Wu, Y.; Shu, C.; Wang, J.; Zhang, H.; Yu, G.; Yuan, J. Analysis of effects of meso-scale reactions on multiphysics transport processes in rSOFC fueled with syngas. *Energy* **2019**, *190*, 116379. [[CrossRef](#)]
39. Barelli, L.; Bidini, G.; Cinti, G.; Ottaviano, A. Study of SOFC-SOE transition on a RSOFC stack. *Int. J. Hydrogen Energy* **2017**, *42*, 26037–26047. [[CrossRef](#)]
40. Luo, Y.; Shi, Y.; Zheng, Y.; Cai, N. Reversible solid oxide fuel cell for natural gas/renewable hybrid power generation systems. *J. Power Sources* **2017**, *340*, 60–70. [[CrossRef](#)]
41. Yu, D.; Hu, J.; Wang, W.; Gu, B. Comprehensive techno-economic investigation of biomass gasification and nanomaterial based SOFC/SOEC hydrogen production system. *Fuel* **2023**, *333*, 126442. [[CrossRef](#)]

42. Zhang, B.; Wang, L.; Li, R. Chapter 10—Bioconversion and Chemical Conversion of Biogas for Fuel Production. In *Advanced Bioprocessing for Alternative Fuels, Biobased Chemicals, and Bioproducts*; Hosseini, M., Ed.; Woodhead Publishing Series in Energy; Woodhead Publishing: Sawston, UK, 2019; pp. 187–205. [CrossRef]
43. Van Herle, J.; Membrez, Y.; Bucheli, O. Biogas as a fuel source for SOFC co-generators. *J. Power Sources* **2004**, *127*, 300–312. [CrossRef]
44. Ma, S.; Loreti, G.; Wang, L.; Maréchal, F.; Van Herle, J.; Dong, C. Comparison and optimization of different fuel processing options for biogas-fed solid-oxide fuel cell plants. *Int. J. Hydrogen Energy* **2021**, *47*, 551–564. [CrossRef]
45. Li, N.; Liu, B.; Jia, L.; Yan, D.; Li, J. Liquid biofuels for solid oxide fuel cells: A review. *J. Power Sources* **2023**, *556*, 232437. [CrossRef]
46. Vakkilainen, E.K. Steam Generation from Biomass: Construction and Design of Large Boilers. 2016. Available online: <https://www.scopus.com/inward/record.uri?eid=2-s2.0-85022084416&partnerID=40&md5=3223cd4cf4e1188a7e90bb3d38697a82> (accessed on 15 June 2023).
47. Gandía, L.M.; Arzamendi, G.; Diéguez, P.M.; He, L.; Yang, J.; Chen, D. Chapter 6—Hydrogen from Biomass: Advances in Thermochemical Processes. In *Renewable Hydrogen Technologies*; Elsevier: Amsterdam, The Netherlands, 2013; pp. 111–133. [CrossRef]
48. Marcantonio, V.; Del Zotto, L.; Ouweltjes, J.P.; Bocci, E. Main issues of the impact of tar, H<sub>2</sub>S, HCl and alkali metal from biomass-gasification derived syngas on the SOFC anode and the related gas cleaning technologies for feeding a SOFC system: A review. *Int. J. Hydrogen Energy* **2021**, *47*, 517–539. [CrossRef]
49. Gandía, L.M.; Arzamendi, G.; Diéguez, P.M.; Martínez-Merino, V.; Gil, M.J.; Cornejo, A. Chapter 5—Biomass Sources for Hydrogen Production. In *Renewable Hydrogen Technologies*; Elsevier: Amsterdam, The Netherlands, 2013; pp. 87–110. [CrossRef]
50. Cordiner, S.; Feola, M.; Mulone, V.; Romanelli, F. Three-Dimensional Based Model of a Planar SOFC Fuelled by Biomass Gas. In Proceedings of the International Conference on Fuel Cell Science, Engineering and Technology, Irvine, CA, USA, 19–21 June 2006.
51. Karim, R.; Naser, J. Numerical Modelling of Solid Biomass Combustion: Difficulties in Initiating the Fixed Bed Combustion. *Energy Procedia* **2017**, *110*, 390–395. [CrossRef]
52. Alnaqi, A.A.; Alsarraf, J.; Al-Rashed, A.A. The waste heat of a biofuel-powered SOFC for green hydrogen production using thermochemical cycle; Economic, environmental analysis, and tri-criteria optimization. *Fuel* **2023**, *335*, 126599. [CrossRef]
53. Geis, M.; Herrmann, S.; Fendt, S.; Jeong, H.; Lenser, C.; Menzler, N.H.; Spliethoff, H. Coupling SOFCs to biomass gasification—The influence of phenol on cell degradation in simulated bio-syngas. Part I: Electrochemical analysis. *Int. J. Hydrogen Energy* **2018**, *43*, 20417–20427. [CrossRef]
54. Jeong, H.; Geis, M.; Lenser, C.; Lobe, S.; Herrmann, S.; Fendt, S.; Menzler, N.H.; Guillon, O. Coupling SOFCs to biomass gasification—The influence of phenol on cell degradation in simulated bio-syngas. Part II—Post-test analysis. *Int. J. Hydrogen Energy* **2018**, *43*, 20911–20920. [CrossRef]
55. Osman, A.I.; Deka, T.J.; Baruah, D.C.; Rooney, D.W. Critical challenges in biohydrogen production processes from the organic feedstocks. *Biomass-Converts. Biorefinery* **2020**, *13*, 8383–8401. [CrossRef]
56. Fischer, F.; Hauser, M.; Hauck, M.; Herrmann, S.; Fendt, S.; Jeong, H.; Lenser, C.; Menzler, N.H.; Spliethoff, H. Effect of internal hydrocarbon reforming during coupled operation of a biomass gasifier with hot gas cleaning and SOFC stacks. *Energy Sci. Eng.* **2019**, *7*, 1140–1153. [CrossRef]
57. Li, Y.; Pang, Y.; Tu, H.; Torrigino, F.; Biollaz, S.M.; Li, Z.; Huang, Y.; Yin, X.; Grimm, F.; Karl, J. Impact of syngas from biomass gasification on solid oxide fuel cells: A review study for the energy transition. *Energy Convers. Manag.* **2021**, *250*, 114894. [CrossRef]
58. El-Emam, R.S.; Dincer, I. Thermal modeling and efficiency assessment of an integrated biomass gasification and solid oxide fuel cell system. *Int. J. Hydrogen Energy* **2015**, *40*, 7694–7706. [CrossRef]
59. Radenahmad, N.; Azad, A.T.; Saghir, M.; Taweekun, J.; Abu Bakar, M.S.; Reza, S.; Azad, A.K. A review on biomass derived syngas for SOFC based combined heat and power application. *Renew. Sustain. Energy Rev.* **2020**, *119*, 109560. [CrossRef]
60. Yang, Y.; Du, X.; Yang, L.; Huang, Y.; Xian, H. Investigation of methane steam reforming in planar porous support of solid oxide fuel cell. *Appl. Therm. Eng.* **2009**, *29*, 1106–1113. [CrossRef]
61. Din, Z.U.; Zainal, Z. Biomass integrated gasification–SOFC systems: Technology overview. *Renew. Sustain. Energy Rev.* **2016**, *53*, 1356–1376. [CrossRef]
62. Vollmar, H.-E.; Maier, C.-U.; Nölscher, C.; Merklein, T.; Poppinger, M. Innovative concepts for the coproduction of electricity and syngas with solid oxide fuel cells. *J. Power Sources* **2000**, *86*, 90–97. [CrossRef]
63. Peksen, M. Chapter 8—Multiphysics Modelling of Energy Systems. In *Multiphysics Modelling*; Peksen, M., Ed.; Academic Press: Cambridge, MA, USA, 2018; pp. 211–236. [CrossRef]
64. Peksen, M.; Blum, L.; Stolten, D. Optimisation of a solid oxide fuel cell reformer using surrogate modelling, design of experiments and computational fluid dynamics. *Int. J. Hydrogen Energy* **2012**, *37*, 12540–12547. [CrossRef]
65. Peksen, M.; Peters, R.; Blum, L.; Stolten, D. Numerical modelling and experimental validation of a planar type pre-reformer in SOFC technology. *Int. J. Hydrogen Energy* **2009**, *34*, 6425–6436. [CrossRef]
66. Nguyen, V.N.; Blum, L.; Peters, R. Operational behavior and reforming kinetics over Ni/YSZ of a planar type pre-reformer for SOFC systems. *Int. J. Hydrogen Energy* **2014**, *39*, 7131–7141. [CrossRef]
67. Nguyen, V.N.; Deja, R.; Peters, R.; Blum, L. Methane/steam global reforming kinetics over the Ni/YSZ of planar pre-reformers for SOFC systems. *Chem. Eng. J.* **2016**, *292*, 113–122. [CrossRef]

68. Audasso, E.; Bianchi, F.R.; Bosio, B. 2D Simulation for CH<sub>4</sub> Internal Reforming-SOFCs: An Approach to Study Performance Degradation and Optimization. *Energies* **2020**, *13*, 4116. [[CrossRef](#)]
69. Moon, D.J.; Ryu, J.W. Electrocatalytic reforming of carbon dioxide by methane in SOFC system. *Catal. Today* **2003**, *87*, 255–264. [[CrossRef](#)]
70. Chen, F.; Zha, S.; Dong, J.; Liu, M. Pre-reforming of propane for low-temperature SOFCs. *Solid State Ionics* **2004**, *166*, 269–273. [[CrossRef](#)]
71. Liso, V.; Olesen, A.C.; Nielsen, M.P.; Kær, S.K. Performance comparison between partial oxidation and methane steam reforming processes for solid oxide fuel cell (SOFC) micro combined heat and power (CHP) system. *Energy* **2011**, *36*, 4216–4226. [[CrossRef](#)]
72. Diéguez, P.M.; Martín, J.L.-S.; Idareta, I.; Uriz, I.; Arzamendi, G.; Gandía, L.M. Chapter 18—Hydrogen Hazards and Risks Analysis through CFD Simulations. In *Renewable Hydrogen Technologies*; Elsevier: Amsterdam, The Netherlands, 2013; pp. 437–452. [[CrossRef](#)]
73. Wu, B. Advances in the use of CFD to characterize, design and optimize bioenergy systems. *Comput. Electron. Agric.* **2013**, *93*, 195–208. [[CrossRef](#)]
74. Baraldi, D.; Melideo, D.; Kotchourko, A.; Ren, K.; Yanez, J.; Jedicke, O.; Giannissi, S.; Toliás, I.; Venetsanos, A.; Keenan, J.; et al. Development of a model evaluation protocol for CFD analysis of hydrogen safety issues the SUSANA project. *Int. J. Hydrogen Energy* **2017**, *42*, 7633–7643. [[CrossRef](#)]
75. Saïd, S.A.; Simakov, D.S.; Waseeuddin, M.; Román-Leshkov, Y. Solar molten salt heated membrane reformer for natural gas upgrading and hydrogen generation: A CFD model. *Sol. Energy* **2016**, *124*, 163–176. [[CrossRef](#)]
76. Peksen, M. 3D transient multiphysics modelling of a complete high temperature fuel cell system using coupled CFD and FEM. *Int. J. Hydrogen Energy* **2014**, *39*, 5137–5147. [[CrossRef](#)]
77. Calzolari, G.; Liu, W. Deep learning to replace, improve, or aid CFD analysis in built environment applications: A review. *Build. Environ.* **2021**, *206*, 108315. [[CrossRef](#)]
78. Hassan, H.; Ren, Z.; Zhou, C.; Khan, M.A.; Pan, Y.; Zhao, J.; Huang, B. Supervised and weakly supervised deep learning models for COVID-19 CT diagnosis: A systematic review. *Comput. Methods Programs Biomed.* **2022**, *218*, 106731. [[CrossRef](#)]
79. Usman, A.; Rafiq, M.; Saeed, M.; Nauman, A.; Almqvist, A.; Liwicki, M. Machine Learning Computational Fluid Dynamics. In Proceedings of the 33rd Workshop of the Swedish Artificial Intelligence Society, SAIS 2021, Online, 14–15 June 2021. [[CrossRef](#)]
80. Van Cranenburgh, S.; Wang, S.; Vij, A.; Pereira, F.; Walker, J. Choice modelling in the age of machine learning—Discussion paper. *J. Choice Model.* **2021**, *42*, 100340. [[CrossRef](#)]
81. Wei, H.; Bao, H.; Ruan, X. Perspective: Predicting and optimizing thermal transport properties with machine learning methods. *Energy AI* **2022**, *8*, 100153. [[CrossRef](#)]
82. Miraftebadeh, S.M.; Longo, M.; Foiadelli, F.; Pasetti, M.; Igual, R. Advances in the Application of Machine Learning Techniques for Power System Analytics: A Survey. *Energies* **2021**, *14*, 4776. [[CrossRef](#)]
83. Nti, E.K.; Cobbina, S.J.; Attafuah, E.E.; Opoku, E.; Gyan, M.A. Environmental sustainability technologies in biodiversity, energy, transportation and water management using artificial intelligence: A systematic review. *Sustain. Futur.* **2022**, *4*, 100068. [[CrossRef](#)]
84. Peksen, M.; Peters, R.; Blum, L.; Stolten, D. Design and Optimisation of SOFC System Components using a Trio Approach: Measurements, Design of Experiments, and 3D Computational Fluid Dynamics. *ECS Trans.* **2009**, *25*, 1195. [[CrossRef](#)]
85. Peksen, M.M. Artificial Intelligence-Based Machine Learning toward the Solution of Climate-Friendly Hydrogen Fuel Cell Electric Vehicles. *Vehicles* **2022**, *4*, 663–680. [[CrossRef](#)]
86. Peksen, M.; Spliethoff, H. Optimising pre-reforming for quality r-SOC syngas preparation using artificial intelligence (AI) based machine learning (ML). *Int. J. Hydrogen Energy* **2023**, *48*, 24002–24017. [[CrossRef](#)]
87. Peksen, M. Chapter 2—Multiphysics Modelling of Fluid Flow Systems. In *Multiphysics Modelling*; Peksen, M., Ed.; Academic Press: Cambridge, MA, USA, 2018; pp. 37–75. [[CrossRef](#)]
88. Blum, L.; Deja, R.; Peters, R.; Stolten, D. Comparison of efficiencies of low, mean and high temperature fuel cell Systems. *Int. J. Hydrogen Energy* **2011**, *36*, 11056–11067. [[CrossRef](#)]
89. De Aguiar, P.; Bourguignon, B.; Khots, M.; Massart, D.; Phan-Thau-Luu, R. D-optimal designs. *Chemom. Intell. Lab. Syst.* **1995**, *30*, 199–210. [[CrossRef](#)]

**Disclaimer/Publisher’s Note:** The statements, opinions and data contained in all publications are solely those of the individual author(s) and contributor(s) and not of MDPI and/or the editor(s). MDPI and/or the editor(s) disclaim responsibility for any injury to people or property resulting from any ideas, methods, instructions or products referred to in the content.